Solvothermal Synthesis and Structure of Anhydrous Manganese(II) Formate, and Its Topotactic Dehydration from Manganese(II) Formate Dihydrate

Martin Viertelhaus,[a] Henning Henke,[a] Christopher E. Anson,[a] and Annie K. Powell*[a]

Dedicated to Professor Hartmut Bärnighausen on the occasion of his 70th birthday

Keywords: Manganese / Formates / Solvothermal synthesis / Solid-state reactions

Recrystallization of manganese(II) formate dihydrate from formic acid under solvothermal conditions results in single crystals of anhydrous manganese(II) formate $Mn(O_2CH)_2$, and the structure of this phase has been determined by X-ray diffraction. The same product can be obtained by solid-state dehydration of single crystals of manganese formate dihydrate, giving crystals that, although of poor quality, still allow for a single crystal structure determination. The structural relationship between the hydrated and anhydrous phases and the nature of the transformation have been determined. Given the nature of the rearrangement involved in the solid-state reaction, it is remarkable that a crystalline product is obtained. Magnetic measurements of the anhydrous manganese(II) formate show it to be a three-dimensional antiferromagnet.

Introduction

Carboxylate-bridged polynuclear manganese complexes have been investigated for many years, particularly with regard to their magnetic properties. Examples include the oxo-centred trinuclear complexes[1] as well as $[Mn_{12}O_{12}(O_2CCH_3)_{16}(OH_2)_4]\cdot 4(H_2O)\cdot 2(CH_3CO_2H)$[2] and its related clusters synthesized with other carboxylic acids[3] which show the behaviour characteristic of "single molecule magnets". In addition to the interest in polynuclear clusters, much research on framework structures produced hydrothermally with carboxylates and related donors has been performed.[4] In this context and relevant to the work presented here the structures of anhydrous manganese acetate and manganese nitrate have only been determined relatively recently[5,6] whereas, for example, the structure of manganese carbonate[7] was determined in the early days of X-ray crystallography. In the course of our work on substitution of acetate ligands with formate, we have developed a new synthetic route to the preparation of crystalline anhydrous metal(II) formates.

With the exception of the strontium salt,[8] all the dihydrated metal(II) formates so far reported form an isomorphous series,[9] and isostructural mixed-metal formate dihydrates have also been described.[10] However, anhydrous diformates are only known for copper and cadmium formate.[11,12] These are synthesized at temperatures around 60−80 °C by slow evaporation of the solvent consisting of a mixture of water and formic acid. Other anhydrous formates are not available using this synthetic route.

Although scientific interest in metal(II) formate dihydrates has increased since they have been used as precursors for dehydrogenation catalysts,[13] very little is known about the structures of the anhydrous salts. With the knowledge of the synthesis and structures of the anhydrous formates, new types of metal oxide catalysts made from these formates are possible. With their increased density these anhydrous salts are more closely related to oxides than the dihydrates. The open framework structures of the precursors which are observed for other anhydrous formates (Mg, Fe, Co, Ni, Zn) are likely to influence the catalytic activity.

Even though metal formate dihydrates are model compounds for hydration/dehydration experiments and their decomposition properties have been well documented,[14] their dehydration products have only been characterized by X-ray powder diffraction (Mg,[15] Mn,[16] Fe,[17] Zn[18]), and their structures are not known. The dehydration of nickel and cobalt formate dihydrate only results in amorphous products.[19,20] However, the rehydration of the dehydrated product of manganese formate dihydrate has been reported and is reversible.[14a]

Using solvothermal conditions we have been able to synthesize a range of previously unreported anhydrous formates (Mg, Fe, Co, Ni, Mn, Zn) as crystalline products. We describe here the structure of anhydrous manganese(II) formate, as well as its formation by a remarkable solid-state dehydration reaction of the dihydrate.

[a] Institut für Anorganische Chemie, Universität Karlsruhe, Engesser Str. 15, Gebäude 30.45, 76128 Karlsruhe, Germany
Fax: (internat.) + 49-(0)721/608-8142
E-mail: powell@achpc50.chemie.uni-karlsruhe.de

Results and Discussion

Recrystallisation of manganese(II) formate dihydrate (MnFD) from formic acid under solvothermal conditions yields pale pink needle-shaped crystals of anhydrous manganese(II) formate (MnFA), suitable for X-ray diffraction (Scheme 1). The structure was determined at 200 K, and crystallographic details are summarised in Table 3. Under ambient conditions the same product in polycrystalline form can be obtained from concentrated formic acid.[21]

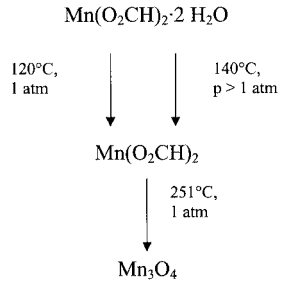

Scheme 1

Anhydrous manganese formate crystallizes in the orthorhombic space group *Pnca* (no. 60) with lattice parameters $a = 5.8127(8)$, $b = 7.509(2)$ and $c = 9.492(1)$ Å and $Z = 4$ (see Table 3). Although MnFA crystallises with an orthorhombic unit cell, while MnFD is monoclinic, inspection of the unit cell parameters shows that two of the three cell lengths are rather close to *b* and *c* for MnFD (Table 3). Since it was soon apparent that the two structures are indeed related (vide infra), and that MnFA can also be obtained via a solid-state dehydration of MnFD, the structure of MnFA was determined in the non-standard setting *Pnca* of the space group *Pbcn* (no. 60) in order to permit consistent labelling of the unit cell axes between the two structures. As the reported structure of MnFD was determined at ambient temperature,[22] we redetermined the structure of MnFD at 200 K, in order to make meaningful comparisons between the two structures.

The asymmetric unit of MnFA contains one independent manganese cation on the special position 4*c* on the twofold axis and one formate group $HCOO^-$ on the general position 8*d*. The coordinating oxygen atoms of the formate ligand differ with respect to their linkage. While O(1) forms μ_2-oxygen-bridges between neighbouring manganese centres, O(2) is monocoordinate. The Mn is coordinated by four O(1) atoms, with the remaining two *cis*-positions occupied by O(2) atoms. This results in the formation of infinite chains of Mn centres linked by pairs of μ_2-oxygen-bridges along **a**, as shown in Figure 1. The coordination spheres around the Mn cations can be described in terms of chains of edge-sharing octahedra. These chains are organized in a manner similar to $ZrCl_4$,[23] in particular with regard to local symmetry elements, with the metal atoms on twofold

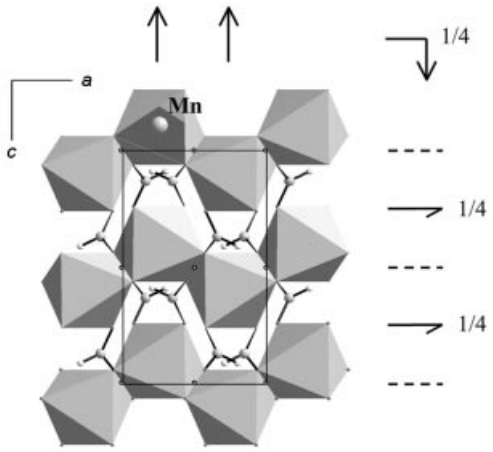

Figure 1. Projection of the structure of MnFA along *b* showing the edge-connected zig-zag chains of octahedrally coordinated Mn atoms; some of the symmetry elements of the space group *Pnca* (no. 60) are given as a help

axes and with inversion centres at the midpoint of the shared edges between octahedra. Similar chains are found in $TcCl_4$.[24] If the structure is viewed along the **a** axis, a rhomboidal network of Mn centres linked via *anti*,*anti*-bridging formate ligands is the characteristic motif (Figure 2). The Mn−O(1) distances in the μ_2-bridges are 2.231(2) and 2.210(2) Å, while the monocoordinate Mn−O(2^{II}) distance is 2.138(2) Å, shorter than in the bridges as might be expected. Bond lengths and angles are listed in Table 1.

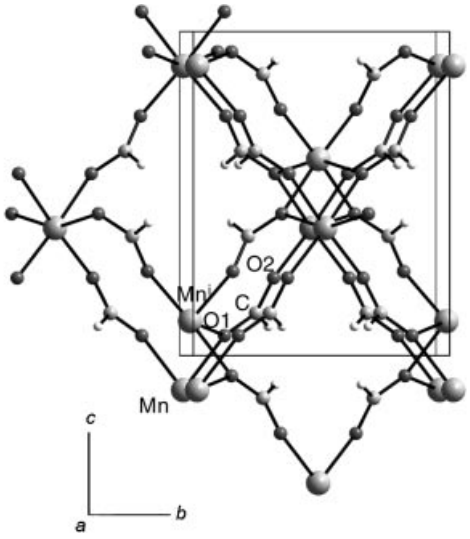

Figure 2. The network of formate groups connecting the manganese atoms of anhydrous MnFA. To aid the comparison with Figure 3 the drawing is slightly rotated with respect to *c*. Due to this rotation, all formate links at heights close to $x = 1/4$ and $x = 5/4$ appear doubled around the octahedrally coordinated manganese chain in the middle of the cell. With reference to Figure 3 the manganese atoms are shifted by 1/4 along *a* owing to the convention that a centre of inversion defines the origin. As a consequence Mn^i is related to Mn by $1 - x, -y, -z$.

Table 1. Bond lengths and angles of MnFA
Symmetry codes: (i) $1 - x, -y, -z$; (ii) $x, 1/2 - y, -1/2 + z$; (iii) $1/2 - x, 1/2 + y, 1/2 + z$; (iv) $1/2 - x, -1/2 + y, -1/2 + z$; (v) $-1/2 + x, y, -z$; (vi) $1/2 - x, -y, z$

Bond lengths [Å]		Bond angles [°]	
Mn−O(1)	2.231(1)	O(2^{iv})−Mn−O(2^{ii})	93.86(10)
Mn−O(1^{i})	2.210(2)	O(2^{iv})−Mn−O(1^{v})	90.80(7)
Mn−O(2^{ii})	2.138(2)	O(2^{iv})−Mn−O(1^{i})	104.27(7)
O(1)−C	1.269(3)	O(1^{i})−Mn−O(1^{v})	158.01(9)
O(2)−C	1.236(3)	O(2^{iv})−Mn−O(1)	176.95(6)
C−H	1.00(3)	O(2^{iv})−Mn−O(1^{vi})	88.86(7)
Mn···Mn(i)	3.539(1)	O(1)−Mn−O(1^{i})	74.29(7)
Mn···Mn(iii)	6.052(1)	O(1)−Mn−O(1^{v})	89.85(5)
Mn(i)···Mn(iii)	5.475(1)	O(1)−Mn−O(1^{vi})	88.45(9)

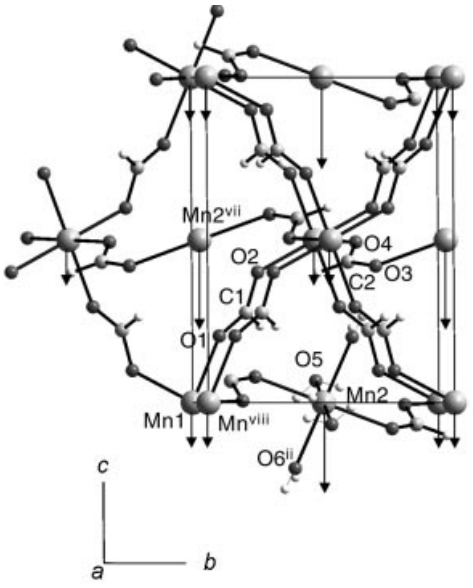

Figure 3. The structure of the dihydrate MnFD for comparison with Figure 2. Apart from the very similar formate-bridged network around atoms of type Mn(1) shown for layer heights close to $x = 0$ and additionally at $x = 1$ in most places, there are Mn(2)-centred loops linking the sheets at $x = 0$ and $x = 1$. Atom Mn(2) at $x = 1/2$ binds to four molecules of crystal water. Arrows indicate the relative moves necessary to reach the structure of MnFA. All equivalents of Mn(2) are shown with the water stripped off. Symmetry codes: (vii): $1 - x, -1/2 + y, 1/2 - z$, (viii): $1 + x, y, z$.

Differential thermal analysis (DTA) and thermogravimetry (TG) studies on MnFD in a nitrogen atmosphere show that the dehydration process takes place in the temperature range from 95 to 135 °C. A continuously decreasing sample mass is observed over this temperature range, with a mass loss of 19.3% (calculated value 19.9% for loss of two waters), and the appearance of an endothermic peak in the DTA curve. The decomposition of MnFA to Mn_3O_4 can be observed between 215 and 260 °C. During the mass loss of 37.4% (calcd. 38.0%) an exothermic peak can be seen in the DTA-curve (Scheme 1).

On dehydration of single crystals of MnFD at 120 °C, their plate-like habit is maintained, but they become off-white and opaque and are frequently cracked. This dehydration event clearly gives rise to a poorer quality sample with much larger spots on the image plate than for the solvothermal crystals. Thus, although the sample still appears to be a single crystal, it in fact consists of a collection of smaller crystallites which are, however, sufficiently aligned to allow for satisfactory structure determination and refinement. This showed that the dehydrated crystals had the identical structure to solvothermally-prepared MnFA, although as expected the final R-factors (Table 3) were higher than for the solvothermally prepared crystals.

A series of X-ray powder diffraction patterns measured during the course of dehydration shows the coexistence of both phases (MnFD and MnFA) (Figure 4). A similar heating experiment during which a sequence of orienting precession photographs was taken of a single crystal at 115 °C, also demonstrates the simultaneous presence of both phases within the same crystal specimen. The sharp diffraction spots of MnFD decrease in intensity while the more diffuse spots assigned to MnFA quickly become stronger. At 120 °C the slightly broadened (0*kl*) reflections of MnFA show clearly the systematic extinctions of the diagonal glide plane. Moreover, these observations give evidence that a fixed spatial relationship exists between the lattice of disappearing MnFD and freshly growing MnFA, indicating a topotactic transformation. Axes **b** and **c** retain their length approximately (see Table 3) and also their orientation within ±0.5°, whereas axis **a** undergoes changes both with regard to the angle of inclination (i.e. β of the monoclinic lattice decreases by over 7° to 90° in the orthorhombic phase) but also more drastically with regard to the shrinkage of the structure.

In contrast to MnFA, MnFD prepared under normal ambient conditions does not form needles, but plates with (100) as the dominant face. In accordance with the habit of the crystals the structure of MnFD consists of layers oriented parallel to the *bc*-plane. Figure 3, the corresponding section suitable for comparison with anhydrous MnFA (cf. Figure 2), shows that in MnFD nets of formate-bridged manganese atoms also exist in a variant similar to that of MnFA (see for instance O(1)−C(1)−O(2) coordinating Mn(1) plus all equivalent units at the same height of $x = 0$). Halfway along the x direction and exactly over the holes of the aforementioned network the other manganese species Mn(2) is surrounded by four water molecules in a planar arrangement. This coordination of Mn(2) is completed by two formate groups lying *trans* to each other (see the equivalent O(3)−C(2)−O(4) in Figure 3) forming crosslinks between the layers in $x = 0$ and $x = 1$. Thus the atom Mn(2) is part of a link extending from the upper left to the lower right of Figure 3.

Although the space group type of MnFD ($P12_1/c1$) is a subgroup of that of MnFA ($P2_1/n2_1/c2/a$), it is not possible that a simple displacive transition is taking place. Instead the mechanism has to be discontinuous due to the loss of the crystal water, causing a dramatic shrinkage of the unit cell along [100]. Whereas in the lower symmetry phase of the dihydrate Mn(1) and Mn(2) both lie on inversion centres, in *Pnca* they are grouped around the centres of inversion necessitating a rearrangement of the structure. The

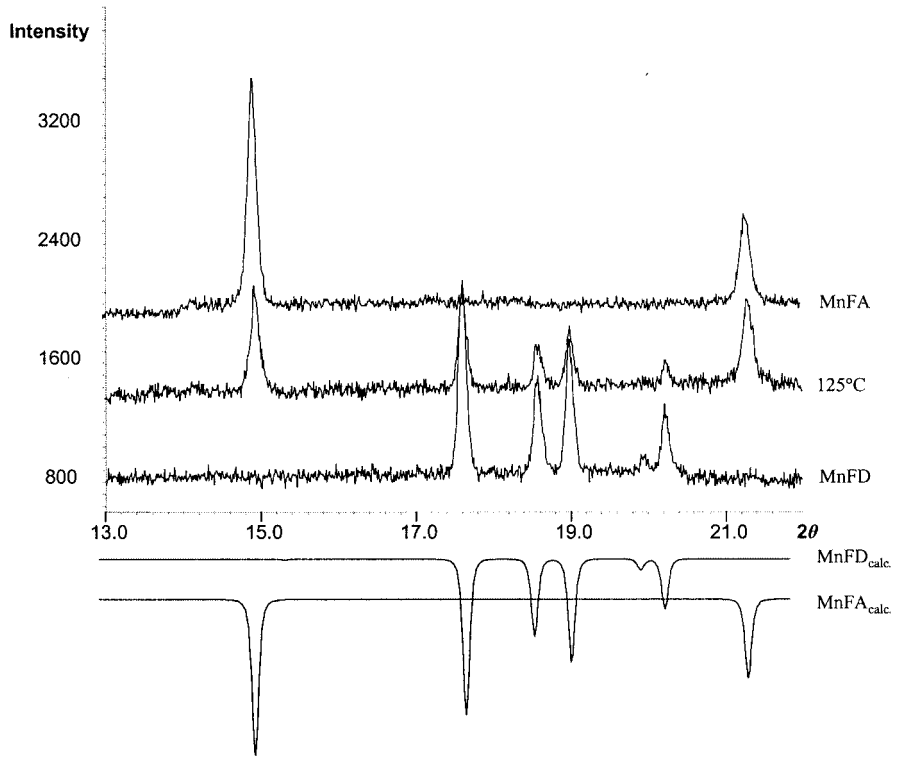

Figure 4. Heating powder diagrams with Cu-$K_{\alpha 1}$ radiation show the coexistence of MnFA and MnFD at an intermediate stage of the dehydration; for comparison the calculated patterns for MnFD and MnFA are given

shorter arrows of Figure 3 merely result from the convention that one of the centres of inversion in MnFA must be chosen to coincide with the origin of the unit cell. As indicated by the longer arrows of Figure 3 the topology of the anhydrous phase in Figure 2 is reproduced by virtue of a transverse move of Mn(2^{vii}) which brings it closer to Mn(1) and Mn(1^{viii}) in the upper and lower layer. The required relative shift in the **c**-direction amounts to ca. 2.77 Å. While in MnFD the distance between Mn(1) and Mn(2^{vii}) is 6.054(2) Å, and between Mn(1^{viii}) and Mn(2^{vii}) 6.917(2) Å, the distance between Mn and Mn^{i} in MnFA, is only 3.539(1) Å (see Table 1). These observations suggest an insertion mechanism on a local scale, which has the advantage that none of the existing bonds to formate groups need to be broken. With loss of the water ligands, the coordinatively-deficient Mn centres −OCHO−Mn(2)−OCHO− reorient themselves to gain additional coordination from formate oxygens O(1) and O(4), which as a consequence are now μ_2-bridging between Mn(1) and former Mn(2) centres, resulting in the zig-zag chains of crystallographically-equivalent Mn centres running along **a** in the structure of MnFA. This process requires a considerable contraction of the MnFD lattice in the **a**-direction amounting to ca. 2.98 Å.

It is remarkable that these large shifts are possible in a topotactical reaction without causing complete destruction of the crystal. As the broad reflections show the anhydrous phase consists of small domains. Their growth seems to start from numerous nucleation sites under the orienting influence of the parent phase MnFD. Similar observations have been reported for the dehydrations of brucite to periclase and of goethite to haematite and magnetite.[25]

Quite naturally nothing can be said by X-ray diffraction about the sequence of steps during the dehydration process. Here the topologies of MnFD and MnFA are simply compared leading to the conclusion that the reaction proceeds topotactically, such that the orientational relationship between both phases is preserved. Although the solid-state process is necessarily reconstructive, it seems to take place surprisingly smoothly.

The IR spectrum of MnFA is simpler than that of MnFD (Table 2); this is consistent with the two structures. Whereas in MnFD there are two inequivalent formate anions in the lattice, and several of the formate vibrational modes give rise to a pair of absorptions, there is only one independent anion in MnFA, and single bands are observed.

Full factor-group analyses for the two IR spectra predict three IR-active modes per formate "molecular" mode in the spectrum of MnFA, and four in the spectrum of MnFD. However, the numbers of observed bands is consistent with the simple molecular analysis.

In addition, there are no absorption bands from water in the MnFA spectrum. The IR spectrum for MnFA corresponds to the spectrum reported by Baraldi[26] for β-MnFA. Baraldi reported this β-MnFA as a metastable phase on the path towards α-MnFA which he identified only by IR spectroscopy. Since we do not observe this α-phase, we cannot say definitively which one is the thermodynamically more stable.

Table 2. Wavenumbers (cm^{-1}) of the IR absorptions for solid MnFD and MnFA (s: strong, w: weak, sh: shoulder, vw: very weak, br.: broad, m: medium)

vibration[27]	MnFD[26]	MnFA
$\nu_{OH,aq}$	3360 s	
	3290 s	
	3220 sh	
$2\nu_4$	2995 vw	3002 w
$\nu_2 + \nu_4$	2940 vw	2935 sh
ν_1, CH stretch	2896 m	2906 m
	2890 vw	
$2\ \nu_5$	2760 w	2783 w
δ_{aq}	1666 w	
ν_4, OCO stretch, asym	1585 s	1602 s
ν_5, OCO deformation, asym	1397 s	1398 s
	1391 s	
	1370 w	
ν_2, OCO stretch, sym	1370 w	1342 s
	1362 s	
ν_6, out-of-plane deformation	1074 vw	1058 vw
ν_3, OCO-deformation, sym	830 w	793 s
	758 s	
γ_{aq}	695 w, br.	
	572 m	

The magnetic behaviour of MnFD has been thoroughly studied.[28] The magnetic susceptibility measurements on MnFA show all the characteristics of a three-dimensional antiferromagnet (Figure 5). The χ^{-1} vs. T plot for temperatures higher than 10 K leads to a Curie temperature Θ of -13.2 K and a Curie constant C of 4.24 emu mol^{-1} K^{-1} which corresponds to the g-factor of 1.97. Every manganese atom has two nearest manganese neighbours along the μ_2-oxygen-bridged chain [3.539(1) Å] and eight further manganese neighbours linked by four *syn-anti* formate bridges [5.475(1) Å] and four *anti-anti* formate bridges [6.052(1) Å]. With its ten direct neighbours the antiferromagnetic coupling of -3.12 cm^{-1} per manganese atom corresponds to an average coupling of -0.31 cm^{-1} $\Theta = 1/3\ S(S+1)\ \Sigma\ J$ with $S = 5/2$ and $\Sigma\ J$ is the sum over all interaction constants for each Mn).

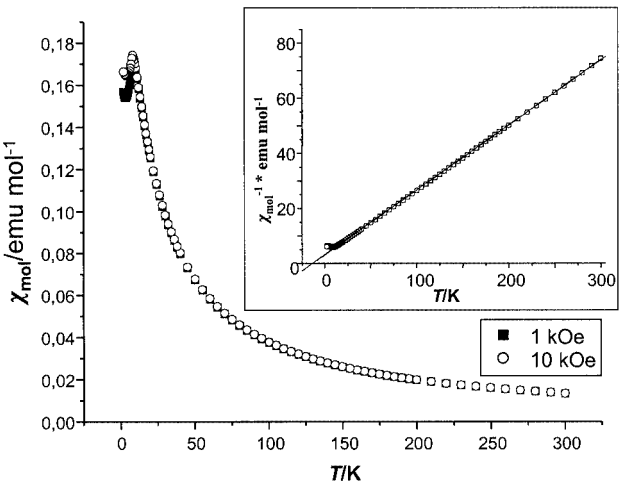

Figure 5. Plot of the magnetic susceptibility, χ_{mol}, of MnFA as a function of temperature in the range of 1.9 to 300 K; the inset shows a plot of χ_{mol}^{-1} versus T

Table 3. Crystal data and details of structure refinement

	MnFD	MnFA	MnFA[a]
Formula	$C_2H_6MnO_6$	$C_2H_2MnO_4$	$C_2H_2MnO_4$
Molecular weight	181.00	144.97	144.97
Crystal system	monoclinic	orthorhombic	orthorhombic
Space group	$P2_1/c$ (no. 14)	*Pnca* (no. 60)[b]	*Pnca* (no. 60)[b]
Temperature [K]	200±1	200±1	200±1
a [Å]	8.7882(18)	5.8127(8)	5.826(5)
b [Å]	7.2164(17)	7.5093(16)	7.549(7)
c [Å]	9.578(2)	9.4923(14)	9.565(10)
β [°]	97.64(3)	90[c]	90[c]
Volume [Å^3]	602.1(2)	414.33(12)	420.7(7)
Z	4	4	4
D_c [g cm^{-3}]	1.997	2.324	2.289
μ [Mo-K_α] [mm^{-1}]	2.154	3.064	3.018
Crystal size [mm]	0.10×0.20×0.20	0.25×0.20×0.20	0.10×0.20×0.20
Crystal shape	pale pink hexagonal plate with (100) dominant	pale pink block cut from needle along [100]	off-white, opaque plate
2θ range [°]	7.3−52.2	8.6−52.3	6.9−54.1
Reflection measured	2251	3897	632
Independent reflections	1038	402	382
R_{int}	0.0289	0.0506	0.0491
observed reflections [$I > 2\sigma(I)$]	856	341	262
wR_2 (all data)	0.0793	0.0833	0.1857
Goodness of fit	1.056	1.059	1.062
R_1 [$I > 2\sigma(I)$]	0.0273	0.0292	0.0568
parameters	109	37	28
max. diff. peak/hole [e·Å^{-3}]	+0.349/−0.303	+0.381/−0.373	+0.812/−0.723

[a] MnFA obtained by dehydration of a single crystal. [b] Non-standard setting of *Pbcn* (no. 60) (see text). [c] For symmetry reasons.

With reference to *J*-values, which are reported for Mn−O(R)−Mn ($J = -1$ to $-5\ cm^{-1}$)[29] and Mn−O−C(R)−O−Mn interactions ($J = -0.2$ to $-0.3\ cm^{-1}$)[30] we can predict that the interactions between manganese atoms within the μ_2-oxygen-bridged chain should be stronger than between adjacent chains. Although the interchain interactions are probably an order of magnitude weaker than the intrachain ones there are four times as many such interactions between the chains as along them, and these may therefore be significant with regard to the three-dimensional antiferromagnetic behaviour. These would require three *J* values and fitting the data in this way would have led to overparametrisation. Antiferromagnetic ordering starts at 8 K, and the spinflop field is 1.2(1) Ts.

Conclusion

We have shown that the crystal structure of anhydrous manganese(II) formate is topotactically related to the structure of manganese(II) formate dihydrate. It can be obtained either by solvothermal reaction or, surprisingly, by the topotactical dehydration of MnFD. Although the μ_2-oxygen-bridges in MnFA lead to one-dimensional chains of oxygen-bridged manganese atoms the additional interchain interactions via formate bridges result in a three-dimensional antiferromagnetic behaviour.

Experimental Section

MnFD was synthesized as reported previously.[16]

Synthesis of $Mn(O_2CH)_2$ (1): $Mn(O_2CH)_2$ was obtained by solvothermal reaction in a steel autoclave with a Teflon-insert of internal volume 10 mL. In a typical experiment $Mn(O_2CH)_2{\cdot}2H_2O$ (0.2 g, 1.1 mmol) was heated in 3 mL of formic acid to 140 °C. During the experiment (88 h) the CO_2 produced as a result of the decomposition of formic acid raises the pressure to such an extent, that in the initial experiment the lid of the Teflon-insert is punctured resulting in the evaporation of the remaining solvent. Subsequently these conditions were reproduced by slightly loosening the autoclave lids to act as a vent in order to avoid damage of the insert. A quantitative yield of needle-like pink crystals of MnFA was obtained. X-ray powder diffraction and TG experiments showed that the product was pure and contained no dihydrate.

X-ray Crystallography: Single-crystal data were measured on a Stoe IPDS image plate area detector diffractometer using graphite-monochromatised Mo-K_α radiation ($\lambda = 0.71073$ Å). Structures were solved by direct methods and refined by full-matrix least-squares against F^2 (all data) using the SHELXTL software package.[31] Non-hydrogen atoms were assigned anisotropic thermal parameters; hydrogen atoms were fully refined with isotropic temperature factors. CCDC-200199 and -200200 contain the supplementary crystallographic data for this paper. These data can be obtained free of charge at www.ccdc.cam.ac.uk/conts/retrieving.html [or from the Cambridge Crystallographic Data Centre, 12, Union Road, Cambridge CB2 1EZ, UK; Fax: (internat.) +44−1223/336−033; E-mail: deposit@ccdc.cam.ac.uk].

Single-crystal photographs were taken on a Buerger precession camera from Huber (Mo radiation). The specimen was heated using a modified Enraf−Nonius FR 559 crystal heater,[32] with which the temperature of the crystal is maintained and controlled by a hot gas stream.

X-ray Powder Diffraction: The X-ray powder patterns were measured on a Stoe STADI P diffractometer using Cu-$K_{\alpha 1}$ radiation (Ge monochromator) and Debye−Scherrer geometry. The sample was placed in an open glass capillary and heated using a Stoe high-temperature attachment.

Thermal Analysis: The differential thermal analysis (DTA) and the thermogravimetry (TG) experiments were carried out using a Netzsch STA 409C system. Samples were heated in Al_2O_3 crucibles with a heating rate of $1\ K\ min^{-1}$ up to 600 °C under a nitrogen atmosphere with flow rate $30\ L\ h^{-1}$.

Susceptibility Measurement: Magnetic measurements were carried out with a Quantum-Design MPMS SQUID magnetometer. The powder sample was placed in a quartz tube and the susceptibility measured in the temperature range from 300 to 1.9 K.

IR Spectroscopy: FTIR spectra were measured using KBr pellets of the sample in the range from 4000 to $400\ cm^{-1}$ with a Perkin−Elmer Spectrum One spectrometer. For each spectrum four scans were measured at a resolution of $4\ cm^{-1}$.

Acknowledgments

We would like to thank PD Dr. Bernd Pilawa for help with the interpretation of the magnetic data.

[1] R. D. Cannon, R. P. White, *Prog. Inorg. Chem.* **1988**, *36*, 195−298.
[2] T. Lis, *Acta Crystallogr., Sect. B* **1980**, 2042−2046.
[3] [3a] H. J. Eppley, H.-L. Tsai, N. de Vires, K. Folting, G. Christou, D. N. Hendrikson, *J. Am. Chem. Soc.* **1995**, *117*, 301−317. [3b] S. M. J. Aubin, Z. Sun, I. A. Guzei, A. L. Rheingold, G. Christou, D. N. Hendrikson, *Chem. Commun.* **1997**, 2239−2240.
[4] [4a] Z. A. D. Lethbridge, A. D. Hiller, R. Cywinski, P. Lightfoot, *Dalton Trans.* **2000**, 1595−1599. [4b] P. A. Prasad, S. Neeraj, S. Natarajan, C. N. R. Rao, *Chem. Commun.* **2000**, 1251−1252. [4c] Z. A. D. Lethbridge, S. K. Tiwary, A. Harrison, P. Lightfoot, *Dalton Trans.* **2001**, 1904−1910.
[5] J. D. Martin, R. F. Hess, *Chem. Commun.* **1996**, 2419−2420.
[6] G. A. Tikhomirov, K. O. Znamenkov, I. V. Morozov, E. Kemnitz, S. I. Troyanov, *Zeitschr. Anorg. Allg. Chem.* **2002**, *28*, 296−273.
[7] R. W. G. Wyckoff, *American Journal of Science* **1920**, *50*, 317−360.
[8] J. L. Galigné, *Acta Crystallogr., Sect. B* **1971**, 2429−2431.
[9] K. Osaki, Y. Nakai, T. Watanabe, *J. Phys. Soc. Jap.* **1963**, *18*, 919.
[10] D. Stoilova, St. Peter, H. D. Lutz, *Zeitschr. Anorg. Allg. Chem.* **1994**, *620*, 1793−1798.
[11] F. Sapina, M. Burgos, E. Escrivá, J.-V. Folgado, D. Marcos, A. Beltrán, D. Beltrán, *Inorg. Chem.* **1993**, *32*, 4337−4344.
[12] G. Weber, *Actc Cryst. Sect. B* **1980**, 1947−1949.
[13] E. Kalalova, V. Ruzicka, *Coll. Czech. Chem. Commun.* **1962**, *27*, 424−429.
[14] [14a] R. C. Eckhardt, P. M. Fichte, T. B. Flanagan, *Trans. Faraday. Soc.* **1971**, *67*, 1143−1154. [14b] Y. Masuda, M. Hatakeyama, *Talanta* **1996**, *43*, 1705−1709. [14c] Y. Masuda, M. Hatakeyama, *Thermochim. Acta* **1998**, *308*, 165−170.
[15] D. Dollimore, J. P. Gupta, D. V. Nowell, *Thermochim. Acta* **1979**, *30*, 339−350.
[16] R. C. Eckhardt, T. B. Flanagan, *Trans. Faraday Soc.* **1964**, *60*, 1289−1298.

[17] C. Malard, *C. R. Acad. Sc. Paris Ser. C* **1966**, 263, 480−483.
[18] T. Arii, A. Kishi, Y. Kobayashi, *Thermochim. Acta* **1999**, *325*, 151−156.
[19] G. Périnet, *Bull. Soc. franc. Minér. Crist.* **1966**, *89*, 325−328.
[20] T. Arii, A. Kishi, *Thermochim. Acta* **1999**, *325*, 157−165.
[21] V. Z. Vassileva, A. L. Karapetkova, *Bulg. Chem. Commun.* **1995**, *28*, 151−159.
[22] G. Weber, *Zeitschr. f. Krist.* **1982**, *158*, 315−318.
[23] B. Krebs, *Angew. Chem.* **1969**, *81*, 120; *Angew. Chem. Int. Ed. Engl.* **1969**, *8*, 146−147.
[24] M. Elder, B. R. Penfold, *Inorg. Chem.* **1966**, *5*, 1197−1200.
[25] [25a] U. Dahmen, M. G. Kim, A. W. Searcy, *Ultramicroscopy* **1987**, 23, 365−370. [25b] J. Lima-de-Faria, *Acta Crystallogr.* **1967**, 23, 733−736.
[26] P. Baraldi, *Spectrochim. Acta* **1979**, *35A*, 1003−1007.
[27] J. D. Donaldson, J. F. Knifton, S. D. Ross, *Spectrochim. Acta* **1964**, *20*, 847−51.
[28] [28a] P. Burlet, P. Burlet, J. Rossat-Mignod, A. de Combarieu, E. Bedin, *Phys. Stat. Sol.* **1975**, *71*, 675−685. [28b] P. Radhakrishna, B. Gillon, G. Chevier, *J. Phys.: Condens. Matter* **1993**, *5*, 6447−60.
[29] [29a] G. S. Papaefstathiou, R. Vicente, C. P. Raptopoulou, A. Terzis, A. Escuer, S. P. Perlepes, *Eur. J. Inorg. Chem.* **2002**, 2488−2493. [29b] G. Aromí, P. C. Berzal, P. Cames, O. Roubeau, H. Kooijman, A. L. Spek, W. L. Driessen, J. Reedijk, *Angew. Chem.* **2001**, *113*, 3552−3554; *Angew. Chem. Int. Ed.* **2001**, *40*, 3444−3446. [29c] M. D. Carducci, R. J. Doedens;, *Inorg. Chem.* **1989**, *28*, 2492−2494.
[30] V. Tangoulis, G. Psomas, C. Dendrinou-Samara, C. P. Raptopoulou, A. Terzis, D. P. Kessissoglou, *Inorg. Chem.* **1996**, *35*, 7655−7660.
[31] G. M. Sheldrick, *SHELXTL 5.1*, Bruker AXS Inc., Madison, WI, **1997.**
[32] B. Anselment, Dissertation, Universität Karlsruhe, **1986**.

Received December 20, 2002

